A Facile Approach to Defect-Free Vinylene-Linked Benzothiadiazole–Thiophene Low-Bandgap Conjugated Polymers for Organic Electronics

ARTICLE *in* MACROMOLECULES · MARCH 2009

Impact Factor: 5.8 · DOI: 10.1021/ma802779m

4 AUTHORS, INCLUDING:

Jianguo Mei
Purdue University
40 PUBLICATIONS **2,656** CITATIONS
SEE PROFILE

Nathan C Heston
California Polytechnic State University, Sa…
9 PUBLICATIONS **321** CITATIONS
SEE PROFILE

Macromolecules

Article

A Facile Approach to Defect-Free Vinylene-Linked Benzothiadiazole#Thiophene Low-Bandgap Conjugated Polymers for Organic Electronics

Jianguo Mei, Nathan C. Heston, Svetlana V. Vasilyeva, and John R. Reynolds

Macromolecules, **Article ASAP** • Publication Date (Web): 17 February 2009

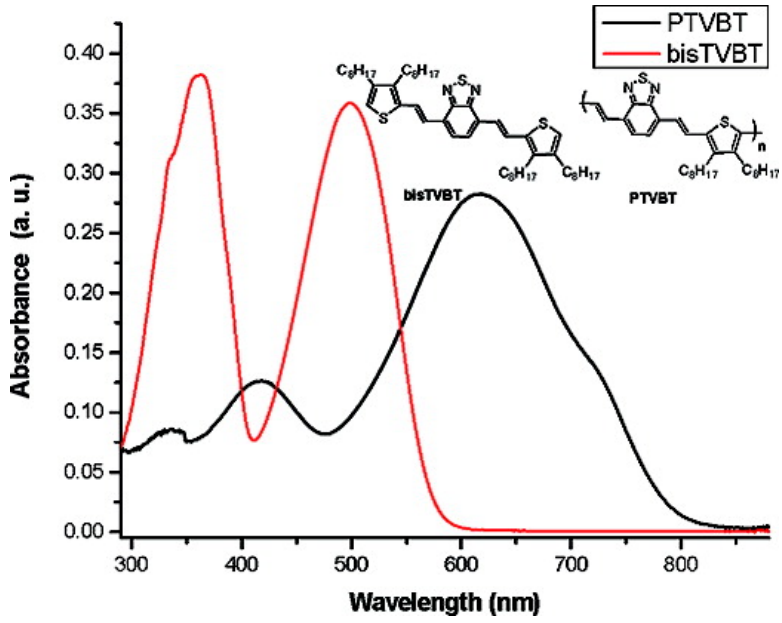

More About This Article

Additional resources and features associated with this article are available within the HTML version:

- Supporting Information
- Access to high resolution figures
- Links to articles and content related to this article
- Copyright permission to reproduce figures and/or text from this article

View the Full Text HTML

A Facile Approach to Defect-Free Vinylene-Linked Benzothiadiazole−Thiophene Low-Bandgap Conjugated Polymers for Organic Electronics

Jianguo Mei, Nathan C. Heston, Svetlana V. Vasilyeva, and John R. Reynolds*

The George and Josephine Butler Polymer Research Laboratory, Department of Chemistry and Center for Macromolecular Science and Engineering, University of Florida, Gainesville, Florida 32611-7200

Received December 13, 2008; Revised Manuscript Received January 19, 2009

ABSTRACT: A facile approach to synthesize vinylene-linked donor−acceptor conjugated polymers is reported and can now be considered for general use. This approach led to a low-bandgap, structurally defect-free vinylene-linked benzothiadiazole−thiophene (PTVBT) polymer and its corresponding model compound bisTVBT using a set of three reactions: Heck coupling, Hunsdiecker reaction, and Suzuki coupling reaction. The polymer and the model compound were fully characterized by ^{1}H and ^{13}C NMR, IR, and elemental analysis. GPC revealed that the number-average molecular weights of PTVBT ranged from 20 000 to 31 000 Da and polydispersity indices from 1.7 to 2.4. Thermal analysis demonstrated that the polymer was stable up to 380 °C under nitrogen without decomposition. Spectroelectrochemical results showed the PTVBT had an optical bandgap of 1.5 eV and was both p- and n-type dopable. The energetic positions of the band edges were determined by cyclic voltammetry and differential pulse voltammetry and suggested that the polymer had a HOMO level at 5.2−5.4 eV, as well as a LUMO level at 3.5−3.6 eV, which renders a strong tendency for photoinduced charge transfer to fullerene acceptors. The polymer has been investigated as an electron donor in photovoltaic devices in blends with PCBM ([6,6]-phenyl C_{61}-butyric acid methyl ester) as an electron acceptor. Power conversion efficiencies ~0.2−0.3% have been obtained with an open-circuit voltage (V_{oc}) of 0.61 V and a short-circuit current density (I_{sc}) of 1.6 mA/cm^2. The relatively low conversion efficiencies may result from low content of polymer in the blends and phase separation as revealed by AFM studies.

Introduction

Low-bandgap donor−acceptor alternating conjugated polymers have received considerable interest as active materials for organic photovoltaics (OPVs), light-emitting diodes (OLED), and electrochromic devices.[1−4] Typical donor−acceptor conjugated polymers are made of electron-deficient nitrogen-containing aromatic heterocycles (2,1,3-benzothiadiazole, [1,2,5]-thiadiazolo[3,4-*g*]quinoxaline, and benzo[1,2-*c*;3,4-*c*]bis[1,2,5]-thiadiazole, etc.) as effective acceptors and electron-rich derivatives (thiophene, alkxoybenzene, carbazole, and fluorene, etc.) as donors.[5−7] Vinylene-linked donor−acceptor (VDA) conjugated polymers are low-bandgap polymers that have a vinylene linkage between the donor and acceptor groups. An advantage of incorporating these vinylene linkages is that they serve to planarize the polymer backbone by eliminating torsional interactions between donor and acceptor rings, thus extending conjugation length, which could lead to a decreased bandgap. In addition, the introduction of these vinylene groups into the polymer backbones provides rotational flexibility which partially increases polymer solubility, allowing chromophore concentration to be increased (defined as the molecular weight ratio of conjugated backbone to solubilizing side chains).[8]

Currently, this class of polymers is still largely unexplored, in contrast to the extensive studies of fully heterocyclic donor−acceptor alternating conjugated polymers. This is perhaps, to a great extent, due to the synthetic challenges. The well-established Gilch and Witting−Horner routes to poly(*p*-phenylenevinylenes) (PPVs) and poly(9,9-dialkylfluorenyl-2,7-vinylenes) (PFVs) are not suitable for VDA conjugated polymers,[9−11] since the above-mentioned acceptors are usually prone to decompose under strong basic conditions. Stille coupling reaction of dibromoaryl compounds with commercially available (*E*)-1,2-bis(tributylstannyl)ethene is also used to prepare poly(arylenevinylenes).[12] However, to put bis(stannylvinyl) functional groups on either a donor or an acceptor is not an easy task. Only a few bis(stannylvinyl)arylene compounds have been reported through hydrostannation.[13] Very recently, a boron-protected haloalkenylboronic acid building block has been reported, which provides a possibility to install a vinylboronic acid functional group.[14] This potential Suzuki polymerization route still has a drawback that vinylboronic acid derivatives are usually unstable.[15] An alternative means to overcome the problem has been reported by preparing PPVs via making bromovinylarylene derivatives.[16−18] However, this method has not been extendable to prepare VDA conjugated polymers. A notable approach in the literature to VDA conjugated polymers is to use Heck polymerization.[19−21] Unfortunately, the Heck reaction is notoriously known for producing structural α-vinyl cross-coupling defects,[22,23] which even in small amount play a detrimental role in organic optoelectronic devices.[24]

In this work, we report a facile approach to prepare defect-free VDA conjugated polymers. The polymers have a higher degree of repeat unit purity in comparison to vinylene-linked polymers prepared via other chemistry (e.g., Gilch or Heck reactions). The vinylene-linked benzothiadiazole−thiophene (PTVBT) polymer has been chosen to demonstrate this chemistry. For the purpose of structural elucidation, its model compound bisTVBT has also been prepared. Electrochemical studies were performed and photovoltaic cells were fabricated by using PTVBT in such a way that VDA conjugated polymers exhibit their potential capabilities as active materials for organic electronics.

Results and Discussion

Polymer and Model Compounds Synthesis. The synthesis of PTVBT is shown in Scheme 1. Heck coupling of 4,7-dibromobenzo[*c*][1,2,5]thiadiazole (**1**) directly with acrylic acids afforded compound **2** in 65% yield. Compound **2** was poorly

* Corresponding author. E-mail: reynolds@chem.ufl.edu.

10.1021/ma802779m CCC: $40.75

Scheme 1. Synthesis of PTVBT

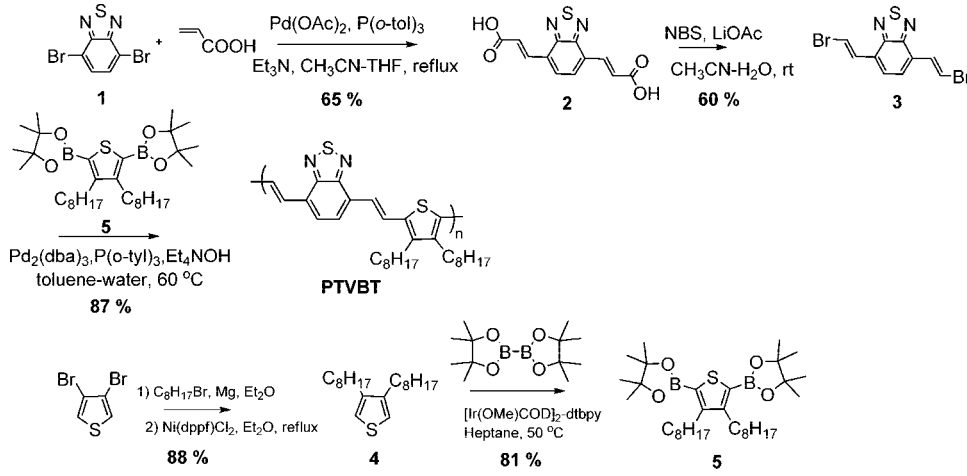

soluble in most common solvents, except THF, DMF, and DMSO, which makes it difficult to purify through chromatography. Fortunately, its triethylamine salt was soluble in water. Hence, the purification of compound **2** was readily achieved by forming the triethylamine salt, following by acidification with aqueous HCl. The catalytic Hunsdiecker reaction of compound **2** with *N*-bromosuccimide in the presence of lithium acetate as catalyst afforded compound **3** in 60−64% yield as light yellow crystals, which appear to be green fluorescent. Low yield or no reaction was noticed when triethylamine or potassium acetate was used instead of lithium acetate. In addition, the choice of solvents played a critical role in this reaction. It turned out that a mixture of acetonitrile and water gave the best results when their volume ratio was around 20−25%, while it was usually around 3% for other catalytic Hunsdiecker reactions in the literature.[25] Compound **5** was obtained in 71% overall yield through two steps. Kumada reaction of 3,4-dibromothiophene with 1-bromooctane gave compound **4** in 88% yield, which after Ir-catalyzed borylation afforded compound **5** in 81% yield.[26] PTVBT was prepared by a Suzuki polycondensation between compound **3** and **5** in 87% yield after Soxhlet extraction and precipitation.[27] The polymer from the chloroform fraction was soluble in THF, toluene, and chlorinated solvents (>10 mg/mL in chloroform). GPC analysis revealed that PTVBT had number-average molecular weights ranging 20 000 to 31 000 Da and polydispersity indices from 1.7 to 2.4 on the base of batch to batch. As a model compound, bisTVBT was prepared by a similar synthetic route, which can be found in the Supporting Information.

Polymer Characterization. The structure of PTVBT was confirmed by ^{1}H NMR, ^{13}C NMR, IR, and elemental analysis. The ^{1}H NMR of PTVBT is here compared with that of bisTVBT to illustrate the polymer structure (see Supporting Information, Figure S1). The model complex bisTVBT shows a very clear splitting pattern. Two doublets are assigned to two *trans*-vinyl protons, which have a coupling constant of 16.2 Hz. Two singlets (7.50 and 6.84 ppm) are evident from the protons on the benzothiadiazole and thiophene rings, respectively. The ^{1}H NMR of PTVBT appears broad at room temperature and even at 60 °C, a feature common to high molecular weight polymers. In addition, the existence of strong polymer aggregation in solution is also responsible for NMR broadening. When heated to 100 °C in deuterated tetrachloroethane, the ^{1}H NMR of PTVBT clearly exhibits three broad, but distinguishable, signals among 7.2−8.5 ppm, corresponding to H_b, H_a, and H_c in the model complex. It is worth mentioning that no ^{1}H NMR signals are found in the region of 5.0−6.0 ppm, where the ^{1}H NMR signals of 1,1-diarylenevinylene defects (α-vinyl coupling defects) usually appear in Heck polymerization.[22] The presence of the *trans*-vinylene functionality is also confirmed by the appearance of FT-IR bands at 955 and 947 cm^{-1} for bisTVBT and PTVBT (see Supporting Information, Figure S2), respectively. These bands are due to the out-of-plane C−H bending of *trans*-vinylene linkages.[22,28]

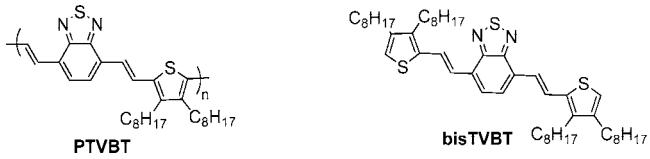

Figure 1. Chemical structures of PTVBT and bisTVBT.

Thermogravimetric analysis (TGA) was carried out to evaluate the thermal stability of PTVBT. A mass loss of 5% is defined as the threshold for thermal decomposition. PTVBT demonstrated good thermal stability with an onset of decomposition at 380 °C. Differential scanning calorimetry (DSC) was performed to characterize the thermal transitions of PTVBT. PTVBT exhibited a glass transition-like feature at 100 °C and a broad endothermic transition at 235 °C on the forward sweep of the first DSC heating cycle. No thermal transitions were observed after the first cycle in the range of −100 to 300 °C.

Optical Properties. The absorption spectrum of PTVBT exhibits a significant change in comparison with that of bisTVBT. BisTVBT has a two-band spectrum with absorption maxima at 359 and 499 nm in THF, while PTVBT shows absorption maxima at 416 and 618 nm, as shown in Figure 2. There is a ∼119 nm red shift in the λ_{max} of the low-energy peaks between PTVBT and bisTVBT. In contrast, because of the steric hindrance imparted by the octyl solubilizing groups, only a 60 nm red shift is observed for a directly linked benzothiadiazole−thiophene alternating polymer and its model compoud.[29] More strikingly, PTVBT has a more red-shifted absorption maximum than its analogous polymer with a thienylene linkage, which has a λ_{max} at 602 nm in chloroform.[30] Clearly, the red shift in PTVBT indicates the polymer is highly conjugated through the planarization of the benzothiadiazole and thiophene units along the polymer backbone. The absorption maximum of PTVBT on ITO (see Supporting Information, Figure S3) exhibits another 15 nm red shift compared to its absorption maximum in THF, due to enhanced $\pi-\pi$ interactions in the solid state. In the fluorescence measurement, bisTVBT shows a well-resolved emission spectrum with a maximum at 610 nm (see Supporting Information, Figure S4). The photo-

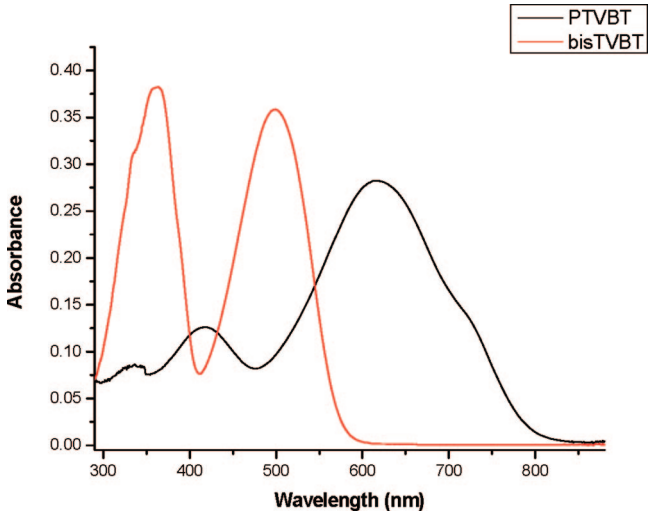

Figure 2. Absorption spectrum of bisTVBT and PTVBT in THF.

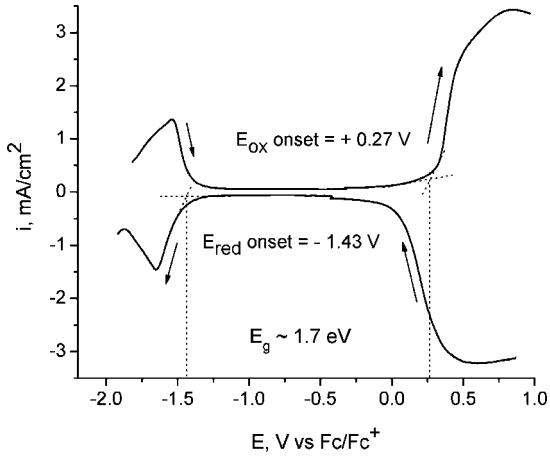

Figure 3. Differential pulse voltammetry of PTVBT on a platinum working electrode in 0.1 M TBAP/PC solution with a step time of 0.02 s, a step size of 2 mV, and amplitude of 100 mV.

luminescence efficiency of bisTVBT was relatively high at 51% compared to that of Rhodamine B in THF. Surprisingly, no fluorescence emission was detected for PTVBT with excitation at 618 nm. Varying the concentration of the polymer solutions yielded no further success. The lack of fluorescence emission can be explained by two facts: the formation of polymer aggregates in solution as illustrated by temperature-dependent ^{1}H NMR study and the low bandgap of PTVBT. The former weakens fluorescence emission through self-quenching, and the latter leads to favorable nonradiative pathways for relaxation of excited states.

Electrochemical Properties. Cyclic voltammetry (CV) and differential pulse voltammetry (DPV) were employed to estimate the HOMO and LUMO levels and the band gap of PTVBT. Electrochemical measurements were performed in an argon-filled drybox in 0.1 M TBAP/PC electrolyte solution for the polymer thin films, which were solution drop-cast on platinum button electrodes. Cyclic voltammograms for the polymer redox processes are presented in the Supporting Information, Figure S5.

Compared to CV, DPV offers better sensitivity and reveals sharper oxidation and reduction potential onsets, which results in an enhanced accuracy when estimating electrochemical band gaps. As illustrated in Figure 3, there is a broad p-type doping process which occurs at potentials in the range of −0.2 to +0.8 V vs Fc/Fc$^+$ with an oxidation onset at +0.27 V, which is more

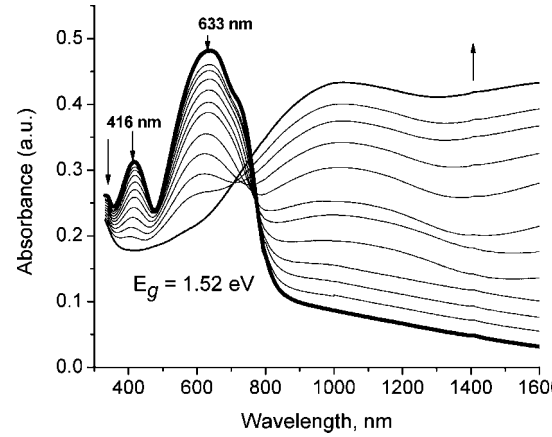

Figure 4. Spectroelectrochemistry of PTVBT spray-cast on ITO/glass from 3 mg/mL solution of the polymer in toluene in 0.1 M TBAP/PC between 0.2 and 0.85 V in 50 mV steps (vs Fc/Fc$^+$). The thick line corresponds to the neutral state of the polymer at 0.2 V.

positive than the onset for the polymer oxidation determined via CV (Figure S5). Based on the electrochemical results, PTVBT showed relatively good air stability. The HOMO energy value was estimated to be between −5.23 and −5.37 eV, based on the assumption that the Fc/Fc$^+$ redox couple is −5.1 eV relative to vacuum.[31] After 100 potential switching cycles at 50 mV s^{-1} between −0.2 and +0.9 V the polymer retained 85% of peak currents. The reductive process was found to be less stable than the oxidative doping; the current of the reduction peak at −1.72 V decreased significantly after the third cathodic scan. The onset for reduction is around −1.43 V and about ∼100 mV more anodic than the corresponding CV reduction onset, indicating a LUMO energy level between −3.55 and −3.61 eV. Hence, the electrochemically determined band gaps of PTVBT are 1.68 eV from CV and 1.76 eV from DPV, respectively.

Spectroelectrochemical measurements can be used not only to determine the band structure of the polymer but also to directly evaluate its electrochromic properties, which is very important from an application standpoint. Figure 4 shows the oxidative spectroelectrochemistry for PTVBT air-brush spray cast on ITO-coated glass electrodes in deoxygenated (via argon purge) 0.1 M TBAP/PC supporting electrolyte solution. The applied potential was increased in 50 mV intervals from +0.2 to +0.85 V vs Fc/Fc$^+$. For the neutral form of the polymer (+0.2 V, thick line in Figure 4) two absorption maxima at 416 and 633 nm were observed, which correspond to the $\pi-\pi^*$ transitions of the polymer and induce a deep blue color in the film. Upon oxidation these transitions vanished with the simultaneous formation of a broad peak outside the visible region at longer wavelengths, associated with low-energy charge carriers (polarons and bipolarons). When the film is completely oxidized (+0.85 V), it is converted into a pale blue color due to the remnant absorption between 600 and 800 nm. The optical band gap (E_g) was determined by the onset of the $\pi-\pi^*$ absorption for the neutral form of the polymer and relatively low around 1.52 eV. After performing oxidative spectroelectrochemical studies no significant degradation of the polymer was observed (7% loss of the anodic and cathodic peak currents of the cyclic voltammograms compared to those of the freshly prepared and switched polymer film). The optically estimated band gap was found to be smaller than electrochemically determined values but remain within a good agreement.

Photovoltaic Properties. Polymer photovoltaic cells were fabricated with a layered structure of glass/ITO/PEDOT:PSS/polymer−PCBM blend/Al (we noted that the use of LiF did not enhance cell fill factors or performance). Characteristic $I-V$ plots of several representative photovoltaic cells with different

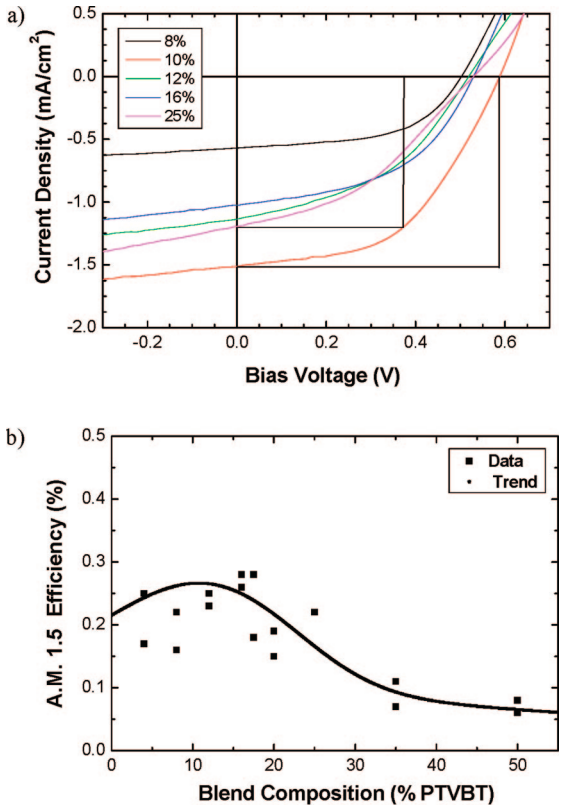

Figure 5. (a) A.M. 1.5 current−voltage characteristics of devices with varied polymer/PCBM weight percentages. (b) A.M. 1.5 efficiencies measured from cells of differing PTVBT−PCBM weight percentages and also differing active layer thicknesses.

PTVBT to PCBM weight percentages are shown in Figure 5a. As is illustrated with the 10% polymer blend cell, fill factors were good and ranged from 33% to 55%. Open-circuit voltages in these cells ranged between 0.5 and 0.6 V. These values are typical for low-bandgap materials.[32,33] Simple metal−insulator−metal models suggest that open-circuit voltages should depend only on the difference between the electrode work functions; however, it is well-known that the polymer HOMO level can influence the maximum open-circuit voltage in polymer cells.[34] Given the low-lying HOMO level of PTVBT, it is possible that further work will result in improved open-circuit voltages. To date, short-circuit current densities are relatively low, at ∼1 mA/cm^2. This is possibly due to blend film morphologies.

Variation of the blend film weight percentage of PTVBT to PCBM resulted in optimal performance with surprisingly low polymer percentages as is illustrated in Figure 5b. Power conversion efficiencies (PCE) mostly fell in the range of 0.2−0.3%. At low polymer percentages the light-absorbing capabilities of the cells could be a limiting factor. Increasing the blend film polymer percentage led to improvement in current densities and overall efficiencies as can be seen in the figures. Upon reaching 10−15% polymer no further improvements in current densities were noted. At higher polymer concentrations we noted a gradual decrease in fill factor resulting in an overall drop in PCE. At just 35% polymer the cell performance dropped by a factor of ∼3. This indicates that light absorption by the polymer was not the performance-limiting factor. The variation in current through the bias voltage sweep remained small, especially at low polymer percentages, indicating good transport properties. IPCE measurements showed a broad absorption following the polymer spectrum, but low overall external quantum efficiencies (see Supporting Information, Figure S6).

Blend film morphologies are possibly the dominant factor limiting photovoltaic performance. Tapping mode AFM measurements revealed a strong correlation between blend film surface morphologies and polymer percentage. A number of differing surface features resulted with small changes in polymer percentages, as shown in Figure 6. With a blend of just 4% polymer and 96% PCBM, the films were very low in rms roughness. When the polymer percentage was increased to 8%, the result was the formation of small, round pits. At 12% polymer many of these pits became quite deep ∼25 nm. Further increases to the polymer percentage led to shallower pits which began to coalesce. At 20%, the morphology appeared to be dominated by multiple small valleys. This effect was much more pronounced at 25% where the valleys deepen and lengthen. These vastly differing morphologies may indicate that the polymer was concentrating at the surface of the anode, an undesirable phase separation that may account for the low IPCE and PCE results.[35] Further work is in progress to establish better photovoltaic performance from these devices.

Experimental Section

Materials and Methods. All reagents and starting materials were purchased from commercial sources and used without further purification, unless otherwise noted. $[Ir(OMe)(COD)]_2$ was stored in a freezer while not in use. Anhydrous solvents were obtained from an anhydrous solvent system. All ^{1}H NMR (300 MHz) and ^{13}C NMR (75 MHz) spectra were recorded on a Varian Mercury 300 spectrometer. Chemical shifts for ^{1}H and ^{13}C NMR were referenced to residual signals from $CDCl_3$ (^{1}H 7.25 ppm and ^{13}C 77.00 ppm) and $C_2D_2C_{l4}$ (^{1}H 6.00 ppm). Mass spectrograms were recorded on either a Finnigan MAT95Q Hybrid Sector (EI, HRMS) or a Bruker Reflex II (MALDI-TOF) mass spectrometer operated in linear mode with delayed extraction. Elemental analyses were carried out by Atlantic Microlab, Inc. UV−vis spectra were recorded on a Varian Cary 500 Scan UV−vis−near-IR spectrophotometer. IR spectra were recorded on Perkin-Elmer Spectrum One FTIR spectrometer. PTVBT and bisTVBT samples were prepared by drop-casting a thin film from tetrahydrofuran (THF) onto a KBr salt plate. Thermogravimetric analysis (TGA) was performed on TA Instruments TGA Q1000 Series using dynamic scans under nitrogen. Differential scanning calorimetry (DSC) analysis was performed using a TA Instruments Q1000 series equipped with a controlled cooling accessory (liquid nitrogen cooling system) at 10 °C/min. Gel permeation chromatography (GPC) was performed at 40 °C using a Waters Associates GPCV2000 liquid chromatography system with an internal differential refractive index detector and two Waters Styragel HR-5E columns (10 μm PD, 7.8 mm i.d., 300 mm length) using HPLC grade THF as the mobile phase at a flow rate of 1.0 mL/min.

Electrochemical Studies. Tetra-*n*-butylammonium perchlorate was synthesized by the metathesis of tetra-*n*-butylammonium bromide (98%, Sigma-Aldrich) and concentrated perchloric acid (≥69%, Fluka). Product was then recrystallized three times from isopropyl alcohol and dried in a vacuum oven for 3 days. Electrolyte salt was transferred to an argon-filled drybox (OmniLab model, Vacuum Atmospheres). Cyclic voltammetry (CV) and differential pulse voltammetry (DPV) studies were performed using an EG&G Princeton Applied Research model 273A potentiostat/galvanostat in an argon-filled drybox. Experiments were carried out in one-compartment electrochemical cell using Ag/Ag^+ reference electrode and platinum foil as a counter electrode; all potentials were reported vs Fc/Fc^+ redox couple. The polymer films were solution drop-cast onto platinum disk electrodes (0.02 cm^2) and switched 20 times at a scan rate 50 mV s^{-1} in the range of potentials between −0.2 and 0.9 V prior to characterization until a complete stabilization of the current responses was reached. The following setup parameters were applied for the DPV studies: a step size of 2 mV, a step time of 0.02 s, and amplitude of 100 mV. For spectroelectrochemical measurements polymer films were air-brush sprayed on ITO-coated glass slides (indium−tin oxide, Delta Technologies, sheet resistance, $R_s = 8-12\ \Omega$) from 3 mg/1 mL solution of PTVBT in toluene and placed in quartz cuvettes of 1 cm path length,

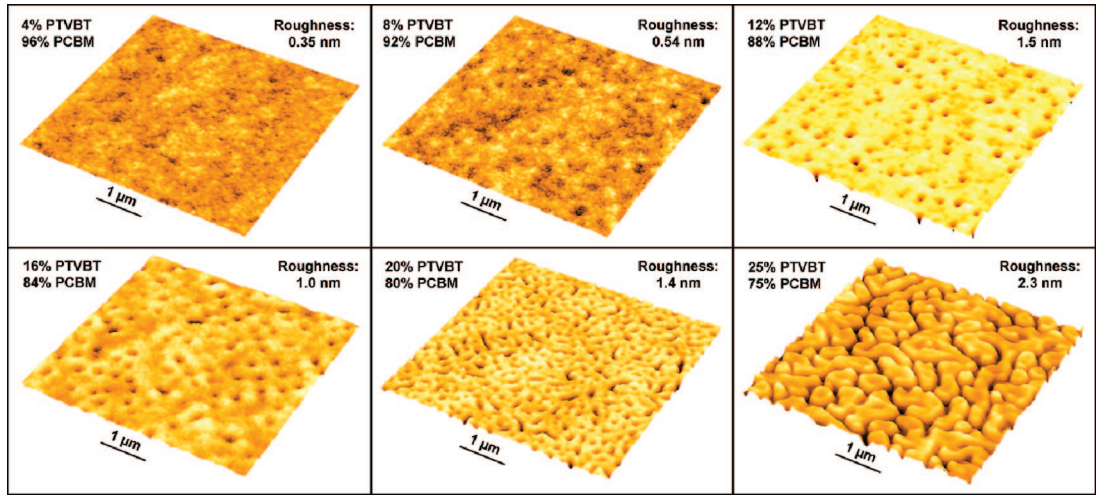

Figure 6. Tapping mode atomic force microscopy images of spin-coated blend films from solutions of varying PTVBT:PCBM weight ratios. The *z*-scale factor is 20.

containing 0.1 M TBAP/PC electrolyte solution. Electrolyte solutions were deoxygenated with argon prior to experiments. A platinum wire was used as counter electrode and a silver wire as quasi-reference electrode (calibrated vs Fc/Fc^+ before and after each experiment).

Fabrication and Characterization of Polymer Solar Cells. Photovoltaic devices were fabricated with the layered architecture: ITO/PEDOT:PSS/PTVBT:PCBM/Al. Fabrication began using patterned indium−tin oxide (ITO)-coated glass substrates (sheet resistance = 15 Ω). The ITO glass was cleaned using cotton swabs and a surfactant solution (∼20 mg of sodium dodecyl sulfate, per 500 mL of DI water) and then sonicated for 15 min in surfactant solution, followed by sonication in Milli-Q filtered deionized water, acetone, and isopropyl alcohol. After removal from the solution, the substrates were dried under nitrogen and treated using an oxygen plasma cleaner (HARRICK PDC-32G) for 15 min. Immediately following the plasma treatment PEDOT-PSS (Bayer Baytron P VP A1 4083) layers were deposited by filtering the PEDOT-PSS solution through 0.20 μm nylon filters and spin-coating at 4000 rpm for 30 s using ∼300 μL of solution. The resulting films are subsequently dried at 110 °C in a vacuum oven for 1 h. Stock (15−20 mg/mL) solutions of PTVBT and PCBM were made in chlorobenzene and stirred overnight inside the inert atmosphere of an argon glovebox. Aliquots of these solutions were combined in different ratios to form blend solutions, which were varied from 4% to 50% PTVBT/PCBM weight/weight. After allowing the blend solutions to stir for a minimum of 6 h, active layers were deposited on top of the PEDOT:PSS layer by spin-coating (500−2000 rpm) for 60 s. The devices were then dried in a vacuum chamber for 6 h. Metal vapor deposition was used to deposit a ∼100 nm aluminum anode at a rate of ∼1.0 Å/s under a vacuum ∼1.0×10^{-6} mTorr.

Device performance was characterized though measurements of incident photon to current efficiency (IPCE) measurements using an Oriel QE/IPCE monochromator, and current−voltage characteristics of the devices were measured at room temperature under A.M. 1.5 irradiation using a Keithley 2400 sourcemeter. Film morphology was explored using a Veeco Innova atomic force microscope in tapping mode in order to investigate the connection between film surface behavior and device performance. Step height measurements were also made using the AFM to determine active layer thicknesses.

(2*E*,2′*E*)-3,3′-(Benzo[*c*][1,2,5]thiadiazole-4,7-diyl)diacrylic Acid (2). To a 250 mL Schlenk flask charged with 4,7-dibromobenzo-[*c*][1,2,5]thiadiazole (5.85 g, 20 mmol), $Pd(OAc)_2$ (2 mol %, 0.8 mmol, 178 mg), and tri(*o*-tolylphosphine) (4 mol %, 1.6 mmol, 488 mg) under argon, the degassed mixture of CH_3CN (120 mL), THF (60 mL), and Et_3N (28 mL, 200 mol) was injected through a septum. The resulting mixture was heated to 60 °C. Acrylic acid (4.32 g, 60 mmol) was then injected slowly. The solids started to disappear, and the solution turned orange. The solution was refluxed at 84 °C for 20 h. The reaction was monitored by TLC. A uniform palladium mirror was formed on the wall of the flask during the period of reaction. While the dark solution was still hot, it was transferred to a clean round-bottom flask (500 mL). The solvent was concentrated on a rotavap. To the concentrated dark viscous mixture was added hexane and diethyl ether (1:1, 200 mL). The resulting precipitates were collected and washed with hexane and diethyl ether mixture. The dark red solids were then dissolved into water (1000 mL, with 7 mL of Et_3N) and stirred for 1 h. The orange solution was filtered, and the filtrate was acidified with 1 M HCl (100 mL) to give orange-yellow precipitates. The precipitates were collected, washed with water, and dried under air overnight. The obtained crude products were dissolved into hot THF (∼300 mL) and filtered. Hexane was then slowly added to the filtrate. The precipitates were filtered and dried under vacuum over 60 °C to afford yellow-orange powder (3.55 g, yield: 65%). ^{1}H NMR (DMF) δ: 12.6 (bs, 2H), 8.16 (s, 2H), 8.13 (d, J = 15.9 Hz, 2H), 7.52 (d, J = 15.9 Hz, 2H). ^{13}C NMR (DMF) δ: 168.6, 154.3, 139.9, 132.3, 129.7, 125.8. HRMS (DIP-CI-MS) Calculated for $C_{12}H_8O_4N_2S$ (M^+): 276.0187. Found: *m*/*z* 276.0205.

4,7-Bis((*E*)-2-bromovinyl)benzo[*c*][1,2,5]thiadiazole (3). To a suspension of (2*E*,2′*E*)-3,3′-(benzo[*c*][1,2,5]thiadiazole-4,7-diyl)-diacrylic acid (5 mmol, 1.38 g) in acetonitrile (50 mL) was added a solution of lithium acetate dihydrate (4 mmol, 408 mg) in water (15 mL). *N*-Bromosuccinimide (10.5 mmol, 1.87 g) was then added. Carbon dioxide gas was observed through bubbler immediately after the addition NBS. The resulting solution was stirred at room temperature for another 2 h after the evolution of gas ceased. Water (100 mL) was added. The yellow-orange precipitates were collected, washed with water, and dried under air. The crude product was then purified by silica gel column chromatography, eluting with CH_2Cl_2/hexane (4:96) to yield light yellow solids (1.10 g, 64%). ^{1}H NMR ($CDCl_3$) δ: 8.01 (d, J = 13.8 Hz, 2H), 7.43 (d, J = 13.8 Hz, 2H), 7.37 (s, 2 H). ^{13}C NMR ($CDCl_3$) δ: 153.1, 133.6, 128.5, 114.5. HRMS (DIP-CI-MS) Calculated for $C_{10}H_7N_2SBr_2$ (M^+): 343.8624. Found: *m*/*z* 343.8618. Anal. Calcd for $C_{10}H_7N_2SBr_2$: C, 34.71; H, 1.75; N, 8.10. Found: C, 34.88; H, 1.59; N, 7.95.

2,2′-(3,4-Dioctylthiophene-2,5-diyl)bis(4,4,5,5-tetramethyl-1,3,2-dioxaborolane) (5). To a 100 mL two-neck flask charged with 3,4-octylthiophene (10 mmol, 2.73 g), 4,4′-di-*tert*-butyl-2,2′-bipyridine (3.0 mol %, 81 mg) and bis(pinacolato)diboron (8 mmol, 2.03 g) were added subsequently under argon. Three cycles of argon−vacuum were then applied. Degassed heptane (50 mL) was injected. $[Ir(OMe)(COD)]_2$ (1.5 mol %, 98 mg) was added under argon, and the mixture was stirred at 50 °C for 16 h. After cooling

down to room temperature, the mixture was filtered and washed with hot hexane. The filtrate was concentrated to yield a viscous oil. The crude product was purified by silica gel column chromatography, eluting with ethyl acetate/hexane (5:95) to give a colorless oil (4.56 mg, 81%). ^{1}H NMR ($CDCl_3$) δ: 2.80 (t, $J = 7.5$ Hz, 2H), 1.56−1.20 (m, 48H), 0.90 (t, $J = 6.3$ Hz, 6H). ^{13}C NMR ($CDCl_3$) δ: 154.3, 83.6, 32.7, 32.2, 30.0, 29.7, 29.6, 28.7, 25.0, 22.9, 14.3. HRMS (APCI-TOF) Calculated for $C_{32}H_{58}B_2O_4S$ ($M + H^+$): 561.4326. Found: *m*/*z* 561.4383. Anal. Calcd for $C_{32}H_{58}B_2O_4S$: C, 68.57; H, 10.43; Found: C, 68.69; H, 10.67.

PBTVT. In a 25 mL flame-dried Schlenk flask, 4,7-bis((*E*)-2-bromovinyl)benzo[*c*][1,2,5]thiadiazole (346.0 mg, 1 mmol), 2,2′-(3,4-dioctylthiophene-2,5-diyl)bis(4,4,5,5-tetramethyl-1,3,2-dioxaborolane) (560.5 mg, 1 mmol), tris(dibenzylideneacetone)dipalladium ($Pd_2(dba)_3$) (13.5 mg, 1.45 mmol %), and tri(*o*-tolyl)phosphine (18.0 mg, 6 mmol %) were dissolved in 12.0 mL of degassed toluene and degassed 20% aqueous tetraethylammonium hydroxide (3.4 mL, 4.25 mmol). The reaction mixture was vigorously stirred at 60 °C for 24 h and then heated up to 95 °C for 6 h. The solution turned from orange to red, dark purple, and finally blue after an hour. After cooling back to 60 °C, 4-iodotoluene (21.8 mg, 0.10 mmol) was added to the mixture. After 2 h, 4,4,5,5-tetramethyl-2-*p*-tolyl-1,3,2-dioxaborolane (21.8 mg, 0.10 mmol) was added, and the reaction was stirred for another 6 h to complete the end-capping reaction. The polymer was purified by precipitation in methanol/water (10:1), filtered through 0.45 μm nylon filter, and purified on a Soxhlet apparatus with methanol, hexanes, and chloroform. To the chloroform fraction was added palladium removal regent (*E*)-*N,N*-diethyl-2-phenyldiazenecarbothioamide (22 mg, 0.1 mmol). The resulting solution was stirred for 2 h. The solution was concentrated under reduced pressure, precipitated in methanol (300 mL), filtered through 0.45 μm nylon filter, washed with methanol, and dried under vacuum at 60 °C overnight to afford PBTVT (432 mg, 87.4%). ^{1}H NMR ($C_2D_2Cl_4$, 100 °C) δ: 8.34 (broad, 2H), 7.62 (bs, 2H), 7.39 (broad, 2 H), 2.4−2.9 (broad, 4H), 1.8−1.20 (m, 24), 0.97 (b, 6H). Anal. Calcd: C, 73.10; H, 8.21; N, 5.68. Found: C, 72.64; H, 8.07; N, 5.67. GPC $M_n = 31\,100$; $M_w = 73\,400$; PDI = 2.36.

Conclusions

We have demonstrated a facile approach to synthesize vinylene-linked donor−acceptor (VDA) conjugated polymers with a method that can find broad applicability for preparing polymers for redox-active and organic electronic applications. Structural α-coupling defect-free low-bandgap PTVBT has been successfully obtained. UV−vis absorption spectroscopy results showed that introducing a vinylene linkage can erase steric hindrance imparted by solubilizing groups and planarize the polymer backbone. Spectroelectrochemistry revealed that PTVBT is an electroactive polymer that can be potentially used in electrochromic devices. The solar cells made of PTVBT:PCBM blends did not give satisfying performance, probably due to low content of PTVBT used in the blend and the unfavorable phase separation observed. Future work will be directed toward using the vinylene chemistry we developed to prepare other vinylene-linked donor−acceptor (VDA) conjugated polymers with less intense interchain interactions for organic solar cells and design VDA materials for near-IR light-emitting diodes.

Acknowledgment. The authors gratefully acknowledge AFOSR (FA9550-06-1-0192) for financial support.

Supporting Information Available: Synthesis of bisTVBT, ^{1}H NMR and IR spectra of PTVBT and bisTVBT, solid-state UV−vis absorption spectrum of PTVBT and PTBVT:PCBM blend, and IPCE curve of polymer cells. This material is available free of charge via the Internet at http://pubs.acs.org.

References and Notes

(1) Bundgaard, E.; Krebs, F. C. *Sol. Energy Mater. Sol. Cells* **2007**, *91*, 954–985.
(2) Kulkarni, A. P.; Zhu, Y.; Jenekhe, S. A. *Macromolecules* **2008**, *41*, 339–345.
(3) Gunbas, G. E.; Durmus, A.; Toppare, L. *Adv. Mater.* **2008**, *20*, 691–695.
(4) Beaujuge, P. M.; Ellinger, S.; Reynolds, J. R. *Adv. Mater.* **2008**, *20*, 2772–2776.
(5) Kitamura, C.; Tanaka, S.; Yamashita, Y. *Chem. Mater.* **1996**, *8*, 570–578.
(6) van Mullekom, H A. M.; Vekemans, J A. J. M.; Meijer, E. W. *Chem.—Eur. J.* **1998**, *4*, 1235–1243.
(7) Zhu, Y.; Champion, R. D.; Jenekhe, S. A. *Macromolecules* **2006**, *39*, 8712–8719.
(8) Feng, X.; Liu, M.; Pisula, W.; Takase, M.; Li, J.; Müllen, K. *Adv. Mater.* **2008**, DOI: 10.1002/adma.200800642.
(9) Becker, H.; Spreitzer, H.; Ibrom, K.; Kreuder, W. *Macromolecules* **1999**, *32*, 4925–4932.
(10) Jin, S. H.; Park, H. J.; Kim, J. Y.; Lee, K.; Lee, S. P.; Moon, D. K.; Lee, H. J.; Gal, Y. S. *Macromolecules* **2002**, *35*, 7532–7534.
(11) Scherf, U. In *Carbon Rich Compounds II, Macrocyclic Oligoacetylenes and Other Linearly Conjugated Systems*; **1999**; pp 163−222.
(12) Hou, J.; Tan, Z.; He, Y.; Yang, C.; Li, Y. *Macromolecules* **2006**, *39*, 4657–4662.
(13) Jung, I.; Lee, T.; Kang, S. O.; Ko, J. *Synthesis* **2005**, 986−992.
(14) Lee, S. J.; Gray, K. C.; Paek, J. S.; Burke, M. D. *J. Am. Chem. Soc.* **2008**, *130*, 466–468.
(15) Roush, W. R.; Brown, B. B. *J. Am. Chem. Soc.* **1993**, *115*, 2268–2278.
(16) Katayama, H.; Nagao, M.; Nishimura, T.; Matsui, Y.; Umeda, K.; Akamatsu, K.; Tsuruoka, T.; Nawafune, H.; Ozawa, F. *J. Am. Chem. Soc.* **2005**, *127*, 4350–4353.
(17) Katayama, H.; Nagao, M.; Nishimura, T.; Matsui, Y.; Fukuse, Y.; Wakioka, M.; Ozawa, F. *Macromolecules* **2006**, *39*, 2039–2048.
(18) Koch, F.; Heitz, W. *Macromol. Chem. Phys.* **1997**, *198*, 1531–1544.
(19) Thompson, B. C.; Madrigal, L. G.; Pinto, M. R.; Kang, T.-S.; Schanze, K. S.; Reynolds, J. R. *J. Polym. Sci., Part A: Polym. Chem.* **2005**, *43*, 1417–1431.
(20) Fu, D.; Xu, B.; Swager, T. M. *Tetrahedron* **1997**, *53*, 15487–15494.
(21) Du, J.; Fang, Q.; Chen, X.; Ren, S.; Cao, A.; Xu, B. *Polymer* **2005**, *46*, 11927–11933.
(22) Grisorio, R.; Mastrorilli, P.; Nobile, C. F.; Romanazzi, G.; Suranna, G. P.; Gigli, G.; Piliego, C.; Ciccarella, G.; Cosma, P.; Acierno, D.; Amendola, E. *Macromolecules* **2007**, *40*, 4865–4873.
(23) Beletskaya, I. P.; Cheprakov, A. V. *Chem. Rev.* **2000**, *100*, 3009–3066.
(24) Johansson, D. M.; Wang, X.; Johansson, T.; Inganas, O.; Yu, G.; Srdanov, G.; Andersson, M. R. *Macromolecules* **2002**, *35*, 4997–5003.
(25) Das, J. P.; Roy, S. *J. Org. Chem.* **2002**, *67*, 7861–7864.
(26) Ishiyama, T.; Takagi, J.; Hartwig, J. F.; Miyaura, N. *Angew. Chem., Int. Ed.* **2002**, *41*, 3056–3058.
(27) Perzon, E.; Zhang, F.; Andersson, M.; Mammo, W.; Inganäs, O.; Andersson, M. R. *Adv. Mater.* **2007**, *19*, 3308–3311.
(28) Pan, M.; Bao, Z.; Yu, L. *Macromolecules* **1995**, *28*, 5151–5153.
(29) Jayakannan, M.; van Hal, P. A.; Rene, A. J. J. *J. Polym. Sci., Part A: Polym. Chem.* **2002**, *40*, 251–261.
(30) Bundgaard, E.; Krebs, F. C. *Macromolecules* **2006**, *39*, 2823–2831.
(31) Thompson, B. C.; Kim, Y. G.; McCarley, T. D.; Reynolds, J. R. *J. Am. Chem. Soc.* **2006**, *128*, 12714–12725.
(32) Wang, X.; Perzon, E.; Mammo, W.; Oswald, F.; Admassie, S.; Persson, N.-K.; Langa, F.; Andersson, M. R.; Inganäs, O. *Thin Solid Films* **2006**, *511−512*, 576–580.
(33) Martijn, M. W.; Mathieu, G. R. T.; Martin, P. S.; Marta, F.; Rene, A. J. J. *Appl. Phys. Lett.* **2006**, *88*, 153511.
(34) Scharber, M. C.; Mühlbacher, D.; Koppe, M.; Denk, P.; Waldauf, C.; Heeger, A. J.; Brabec, C. J. *Adv. Mater.* **2006**, *18*, 789–794.
(35) Smith, A. P.; Smith, R. R.; Taylor, B. E.; Durstock, M. F. *Chem. Mater.* **2004**, *16*, 4687–4692.

MA802779M

Supporting Information:

A Facile Approach to Defect-free Vinylene-linked Benzothiadiazole-thiophene Low Bandgap Conjugated Polymers for Organic Solar Cells

*Jianguo Mei, Nathan Heston, Svetlana V. Vasilyeva, John R. Reynolds**

The George and Josephine Butler Polymer Research Laboratory, Department of Chemistry and Center for Macromolecular Science and Engineering, University of Florida, Gainesville, Florida 32611-7200

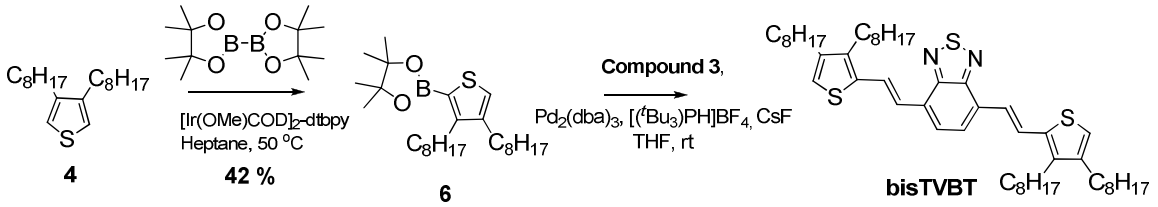

2-(3,4-dioctylthiophen-2-yl)-4,4,5,5-tetramethyl-1,3,2-dioxaborolane (6). To a 25 mL two-neck flask charged with 3, 4-octylthiophene (5.0 mmol, 1.37 g). 4,4'-di-tert-butyl-2,2'-bipyridine (3.0 mol %, 40.2 mg) and bis(pinacolato)diboron (2.8 mmol, 711 mg) were added under argon. Three cycles of argon-vacuum were then applied. Subsequently, Degassed heptane (25 ml) was injected. $[Ir(OMe)(COD)]_2$ (1.5 mol %, 49 mg) was added under argon and the mixture was stirred at 50 ^{o}C for 16 h. After cooling down to room temperature, the mixture was filtered and washed with hot hexane. The solvent was removed and the crude oil product was purified by silica gel column chromatography, eluting with CH_2Cl_2/Hexane (3:7) to give colorless oil (917 mg, 42 %). ^{1}H-NMR ($CDCl_3$) δ: 7.16 (s, 1H), 2.82 (t, J =

7.5 Hz, 2H), 2.54(t, J = 7.2 Hz, 2H),1.62–1.54 (m, 2H), 1.54–1.45 (m, 2H),1.32 (s, 12 H), 1.23–1.29 (m, 20H) 0.87 (t, J = 6.3 Hz, 6H); ^{13}C-NMR ($CDCl_3$) δ: 153.6, 144.1, 127.2, 83.6, 32.2, 32.1, 30.4, 30.0, 29.8, 29.7, 29.65, 29.5, 28.8, 25.0, 22.9, 14.3; HRMS (APCI-TOF) Calculated for $C_{26}H_{47}BO_2S$ (M + H^+): 434.3499. Found: *m/z* 434.3501.

bisTVBT. To a flask charged with 4,7-bis((E)-2-bromovinyl)benzo[c][1,2,5]thiadiazole (1 mmol, 346 mg), $Pd_2(dba)_3$ (2.5 mmol, 23 mg), [(^{t}Bu$_3$)PH]BF_4 (7.5 mol %, 22 mg), CsF (6 mmol, 912 mg) under argon atmosphere, 2-(3,4-dioctylthiophen-2-yl)-4,4,5,5-tetramethyl-1,3,2-dioxaborolane (2.4 mmol) in THF (40 ml) was injected. The resulting mixture was stirred at room temperature for 10 h. Water (100 ml) was added and the organic phase was extracted with diethyl ether (2 x 20 mL). The combined organic phase was dried over $MgSO_4$. The solvent was removed and the crude product was purified by silica gel column chromatography, eluting with Dichloromethane/Hexane (15: 85) to yield red solids (689 mg, 86%). ^{1}H-NMR ($CDCl_3$) δ: 8.38 (d, J = 16.2 Hz, 2H), 7.50 (s, 2H), 7.29 (d, J = 16.2 Hz, 2H), 6.84 (s, 2H), 2.75 (t, J = 6.6 Hz, 4H), 2.55 (t, J = 7.5 Hz, 4H), 1.70–1.20 (m, 48H), 0.90-0.98 (m, 12H); ^{13}C-NMR ($CDCl_3$) δ: 154.0, 143.6, 142.0, 137.8, 129.3, 127.4, 126.2, 123.4, 119.4, 32.2., 32.1, 31.3, 30.0., 29.9, 29.8, 29.7, 29.6, 29.56, 29.5, 29.3, 27.3, 22.9, 14.3; HRMS (APCI-TOF) Calculated for $C_{50}H_{76}N_2S_3$ (M + H^+): 801.5243. Found: *m/z* 801.5210. Anal. Calcd for $C_{50}H_{76}N_2S_3$: C, 74.94; H, 9.56; N, 3.50. Found: C, 75.08; H, 9.56; N, 3.50.

Figure S1. ^{1}H-NMR spectra of **bisTVBT** in deuterated chloroform (top) at room temperature and **PTVBT** in deuterated tetrachloroethane at 100 ^{oC}

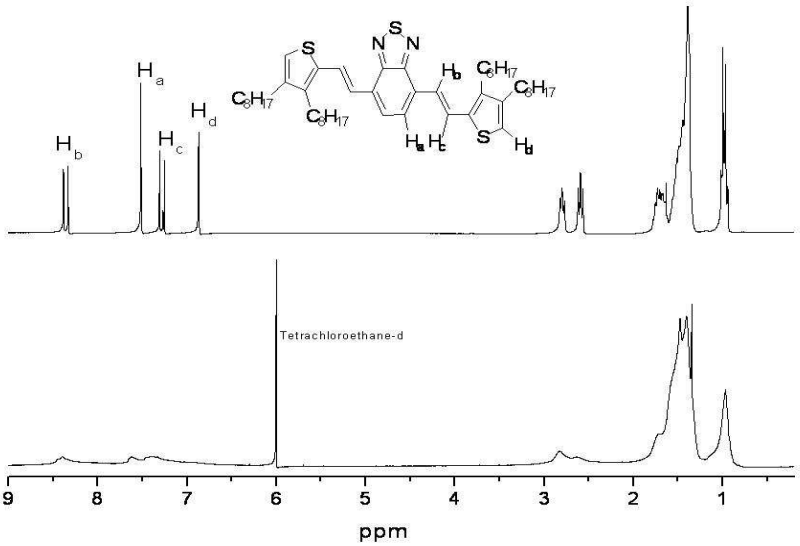

Figure S2. IR spectra of of **bisTVBT** and **PTVBT**

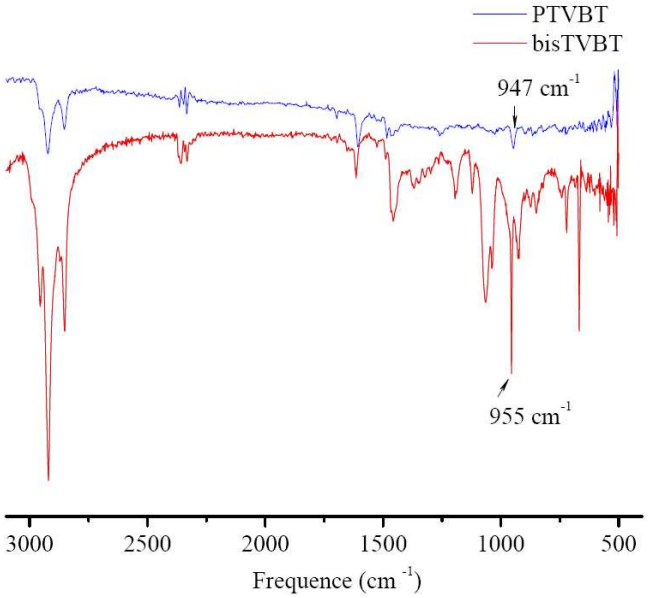

Figure S3. Solid state absorption of PTVBT and PTVBT/PCBM blend on ITO overlaid with the solar simulator spectrum (AM 1.5 conditions, solid line). The Figure shows a great match between the photocurrent spectrum of the blend and the photon emission of the sun.

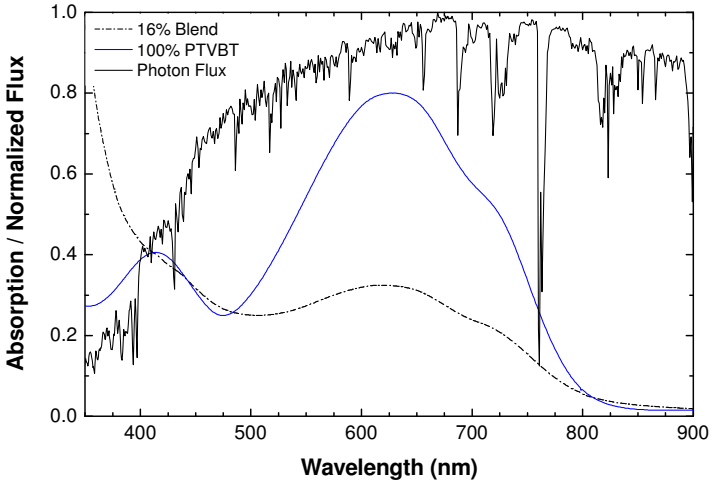

Figure S4. Photoluminescence spectrum of bisTVBT in THF, excited at 470 nm.

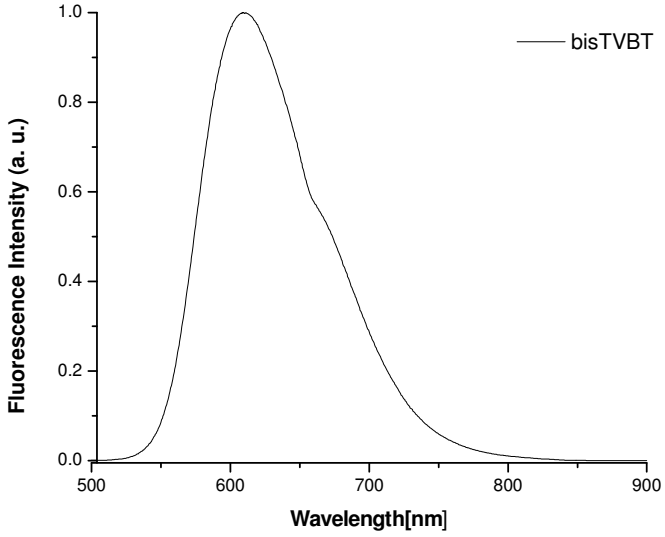

Figure S5. Cyclic voltammetry of PTVBT on a platinum working electrode (0.02 cm^2) in 0.1M TBAP/PC solution at 50mV s^{-1}.

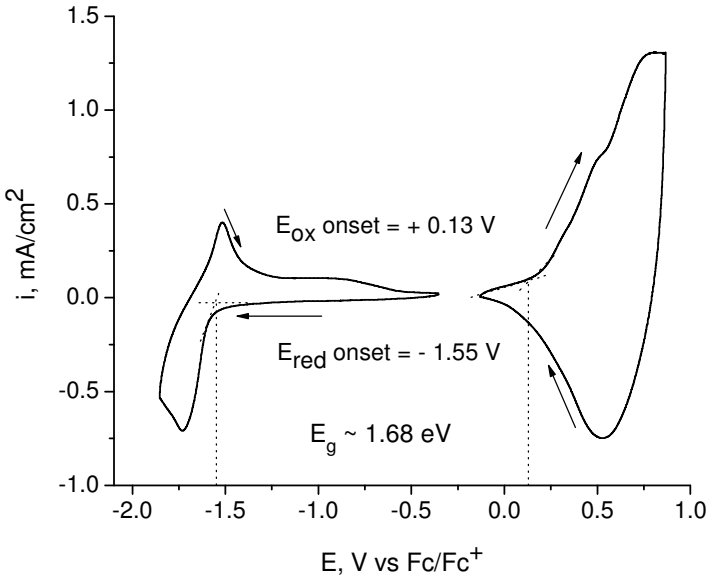

Figure S6. IPCE results for a are displayed for a typical PTVBT cell.